An alternative explanation of forming force reduction for forming process submitted to vibration: Influence of the waveform in the viscoplastic domain

A. Khan [a,d,*], C. Giraud-Audine [b], R. Bigot [a], G. Abba [a], M.Z. Abideen [c]

[a] Laboratoire de Conception, Fabrication, Commande, LCFC EA 4495, Arts et Métiers Paristech-Metz, 4 rue Augustin Fresnel, 57078 Metz Cedex 3, France
[b] Laboratoire de Physique et de Mćanique des Matŕiaux, LPMM, CNRS, Arts et Mĺiers Paristech-Metz, 4 rue Augustin Fresnel, 57078 Metz Cedex 3, France
[c] Pakistan Institute of Engineering and Applied Sciences, PIEAS, 45650 Nilore, Islamabad, Pakistan
[d] Higher Education Commission, HEC, Sector H-9, 44000 Islamabad, Pakistan

A B S T R A C T

This article addresses the effects of vibrations on a viscoplastic workpiece applied during the forging process. To achieve this goal, a phenomenological model based on the slice method combined with a Norton–Hoff viscoplastic law is developed. It allows to study the impact of vibration on the reduction of the mean forging load which has been experimentally observed before, and demonstrates that the sensitivity to strain rate is a key parameter. Moreover, based on the model, a new waveform of the vibrations is proposed that enhance the mean forging load reduction. Finite element simulations and experiments have been performed to evaluate the validity of the model in the case of sinusoidal and triangular waveforms, and are in good agreement with the analytical model's predictions.

Keywords:
Forming process
Vibrations
Viscoplasticity
Load reduction

1. Introduction

Due to the importance of forming processes in the industry and the cost involved, their improvement has long been the aim of the researchers. Different techniques have been applied to reduce the loads applied during forming processes include the use of lubrication, heating of the material and recently incorporating vibrations during forming process. Those solutions influence either friction or material properties.

Lubrication aims at reducing friction. Metal lubricants applied to tool-work interface in many forming operations to reduce the apparent friction coefficient. On one hand, this reduces the sticking at the tool-workpiece interface. As a consequence, the metal flows more easily reducing loads, power and tools wear. It also improves the surface finish and helps to cool the tooling. On the other hand, the lubricant has to be chosen carefully, and its application on the workpiece is crucial. Another limitation in using this solution is the incompatibility of most lubricant with environmental requirement.

Heating of material during forming process is a second technique which directly act on the material properties, as increasing the metal temperature reduces the yield strength and increases ductility. Although every deformation operation can be accomplished with lower forming load and power at high temperature, it affects some very important final material properties such as the surface properties or the crystalline structure.

Finally, a recent technique consists of applying vibrations during the forming process. According to Presz and Andersen (2007), this technique combines advantages of both lubrication and heating of material during forming process while removing all the disadvantages of the two previously discussed techniques. The influence of vibration on metal forming processes can be attributed to two phenomena. First, a rheological effect which could explain the reduction of the yield stress by the influence of vibrations on the dislocation mobility presented by Blaha and Langenecker (1959). This is similar to the advantages of heating the material. Secondly, another effect known as surface effect could take place. Indeed, it is known that the effective coefficient of friction drops with periodic reduction of contact areas and/or periodic change in direction of friction force vector as studied by Lehfeldt (1969). This results in a 'dynamic' lubrication.

One of the earliest application of vibration in metal forming process was reported by Blaha and Langenecker (1959). They used

ultrasonic vibrations during tensile testing of metal crystals. Substantial reduction of the yield stress was reported as soon as ultrasonic vibrations were applied. The proposed explanation was that dislocation displacement was eased by the superimposition of a cyclic loading. Mousavi et al. (2007) have shown that, when applying ultrasonic vibrations, if the extrusion speed is kept below a critical speed, the extrusion load and material flow stresses are reduced. The average extrusion load can equivalently be decreased by reducing the extrusion speed or increasing the amplitude suggesting that only the relative speed is relevant.

The researchers Rosochowska and Rosochowski (2007) studied vibration assisted back extrusion and determined forming force for different die velocities. It was noted that the maximum value of the oscillating forming force is lower than the force under static condition. The difference between the forming force under static condition and the maximum forming force when the tool was subjected to vibrations, decreased with increasing die velocity. A possible explanation of this result is that the vibration reduced the friction force. The influence of ultrasonic vibration both parallel and perpendicular to the sliding direction on sliding friction has been studied by Kumar and Hutchings (2004) for samples of aluminium alloy, copper, brass and stainless steel sliding against tool steel. Experiments were performed at a mean sliding speed of 50 mm s^{-1}, and at mean contact pressures up to 0.7 MPa, with vibration amplitudes up to 10 μm at 20 kHz. Significant reduction of the sliding friction was observed. A numerical study of the effects of radial and axial ultrasonic excitation on an extrusion process has been presented by Lucas and Daud (2009). The study supports experimental findings that the benefits of applying ultrasonic excitation can only be achieved below a defined critical extrusion speed. Aluminum is used as workpiec material with elastic-plastic isotropic with low strain hardening behavior. Reduction in forming load is reported due to the effective reduction during the interval of ultrasonic excitation. Effect of vibration extrusion on the structure and properties of high-density polyethylene pipes (HDPE) has been analyzed by Kaiyuan et al. (2009). Important finding from these research work predicts increase in bursting pressure of pipe, tensile yield strength, higher crystallinity, larger crystal sizes and more perfect crystals which are highly desirable in metal forming process.

Similarly, Siegert and Ulmer (2000) and Siegert and Ulmer (2001) studied vibration assisted wire and tube drawing processes. Applied frequency was in ultrasonic domain f=20–22 kHz and amplitude and velocities were 0–46 μm and 5–340 mm s^{-1}. It was observed that there is reduction in drawing force and also smooth surface was obtained. The effect of applying radial and transverse ultrasonic vibrations on dies was investigated by Murakawa and Jin (2001) and compared with the effect of applying axial ultrasonic vibration and conventional process without vibration. It was verified that radially ultrasonic vibration assisted drawing process is effective in increasing the critical speed in ultrasonic wire drawing by 10 times that conventional axially vibrated dies. Hayashi et al. (2003) reported that the application of ultrasonic vibrations on the dies of tube and wire drawing results in reduction of the forming loads, flow stress, friction between die and work-piece. Better surface qualities, reduction in wrinkling, cracking and higher precision were also reported. Studies also mentioned that the extent to which an oscillation may be advantageous depends upon the material, the drawing speed and the direction of the oscillation relative to that of the drawing. Ashida and Aoyama (2007) noted that there was reduction in friction, wrinkling and cracking when the vibration of frequency (11.4, 19.5 kHz) and amplitude 11.4 μm was applied during the deep forming process.

Polyakov and Mikhailov (1967) performed the experiments to analyze the effect of vibrations on forging process. It consisted in equipping a press with rotating unbalanced inertia. A vibrational load in a frequency range spanning between 10 Hz and 40 Hz was used. The strain obtained at constant load capacity increases by fifty percent and a similar value for the reduction in specific pressure was reported. It was also observed that the tendency of the blank forged to assume a barrel-like shape was reduced indicating that both the stresses and strains are more uniformly distributed. During their work Huang et al. (2000) proposed a finite element model (FEM) to study the effect of vibration during upsetting of an elasto-viscoplatic cylindrical sample of plasticine. Using a Herschel–Bulkley law for the viscoplastic domain and a Coulomb model of the friction forces, the FEM model implemented in ABAQUS was able to reproduce experimental results for vibration in the range of 5–100 Hz, and amplitude varying from 5 to 40 μm. An appreciable decrease in the stress necessary to maintain plastic flow in comparison with that under static load is reported. In a later study, Huang et al. (2002) presented results while upsetting a model paste with ultrasonic vibration superimposed during a static loading. When applying a constant die vibration amplitude of 10 μm and frequency of 20 kHz, an immediate drop in the mean forming load was observed. When the ultrasonic oscillation application interval was longer, further reduction in the forming load was recorded. It was an indication that locally, in the vicinity of the boundary, temperature increases and yield stress reduces in the affected region. During their study, Daud et al. (2007) analyzed the effects of superimposed ultrasonic vibrations (f = 20 kHz, a = 8 μm, v = 5 mm/min and μ = 0.25, 0.001) on tension and compression tests of aluminum. Reduction in mean upsetting/compression force and mean flow stresses was observed. Hung and Hung (2005) analyze the influence of ultrasonic-vibration (f = 20 kHz ± 300 Hz, a = 5.6 μm and v = 5–50 mm s^{-1}) during hot upsetting of aluminum and reduction in compressive loading force and friction between die and workpiece has been observed. Hung et al. (2007) have also carried out experiments to evaluate the frictional effect of ultrasonic-vibration on upsetting for the same process. It was found that there is reduction in mean stresses during the process when vibration is applied. During his research work, Ly et al. (2009) applied low frequency sinusoidal vibration (0–125 Hz) during the upsetting process of plasticine and found the gain in mean forging force reduction.

From the brief review exposed above, it is clear that the influence of using vibrations (both low and high frequencies) on various metal forming processes has been experimentally investigated by several researchers for a while. However, though most of the studies have demonstrated the desirable effects of vibration-assisted forming process, very few have discriminated the origin of the phenomenon involved (rheologic, tribologic or both). Extent to which each of the described mechanism specifically affects a process remains unclear and experimental techniques for isolating these influences have yet to be developed. Moreover, experimental results Ly et al. (2009) show that this effect also exists at low frequencies (0–125 Hz). So far, most of the studies were either experimental or rely on finite elements models. This paper proposes an attempt to explain the reduction of forging load while vibration are applied. Thus in the Section 2, an analytical model will be developed based on some kinematic assumptions and the Norton-Hoff law. Though simple, the model is able to capture the some of the features experimentally such as forging force reduction by application of low vibration in the process as observed by Ly et al. (2009). Moreover, using the model, it will be shown that the choice of the waveform applied can dramatically improve the load reduction. In the following sections, finite element analysis (FEM) and experiments' results will be used to validate the analytical model. For FEM analysis, the parameters used will be chosen as close as possible to the model's assumptions to verify the influence of the kinematic. After FEM simulations, some experimental results will be presented in next section. Plasticine and aluminium were chosen as workpiece materials. Plasticine is chosen because

it's behavior is like hot steel at room temperature. Aluminium 6060 will be used because of the availability of well known raw material and better repeatability. For aluminium 6060 T6, in order to reduce the flow stress of the material, a solution heat treatment was applied to the samples. It consists of heating the workpiece at 550 °C followed by a rapid quenching in cold water. The resulting samples are used immediately to avoid the ageing of the material. The purpose of performing experiments is to see the deviation of analytical model from the real life results. Certain assumptions made during the development of analytical model will also be analyzed in order to verify the robustness of the proposed analytical model and its validity will be discussed.

2. Analytical model

2.1. Method and assumptions

The goal of the model is to predict the forging load in the presence of vibrations applied to the die. The simplest case of the upsetting of a cylindrical workpiece[1] between two rigid platen will be considered. Certain assumptions made in this method are:

- Shape of the workpiece will remain same before and after forging process i.e. cylinder remains cylinder and parallelepiped will be parallelepiped,
- The process is supposed to be isothermal, hence no thermal dependency of the material's property will be considered
- The material is supposed to be purely viscoplastic, and friction is taken into account using a Coulomb model.

If sliding at the interface occurs, the tangential stress τ at the interface reads:

$$\tau = -\mu\sigma_n \tag{1}$$

where μ is the Coulomb coefficient and σ_n is the normal stress at the interface.

The platen are supposed to be rigid, and it will also be assumed that through the displacement of the die the height of the sample $h(t)$ is imposed. Moreover the geometry of the sample is supposed to be conserved during deformation, that is the sample will remain cylindrical and no barelling is considered. Stress is assumed to vary principally in the radial direction, where the material flow occurs, thus stresses will be solely functions of the radius r. Hence one can consider that, in a slab such as represented on Fig. 1, the stresses are constant Lange (1985). The case when sliding occurs at the interfaces is considered. Writing the equilibrium of a slab yields (refer to Fig. 2 for notations):

$$(\sigma_r + d\sigma_r)(r + dr)hd\theta - \sigma_r rhd\theta \quad - 2\sigma_\theta hdr \sin\frac{d\theta}{2} - 2\mu\sigma_n rdrd\theta = 0 \tag{2}$$

Since $d\theta$ is supposed to be small, one can use the approximation:

$$\sin\frac{d\theta}{2} \simeq \frac{d\theta}{2} \tag{3}$$

Moreover, one has:

$$\sigma_\theta = \sigma_r \tag{4}$$

[1] This assumption on the geometry is arbitrary. A parallelepipedic geometry is also simple to study.

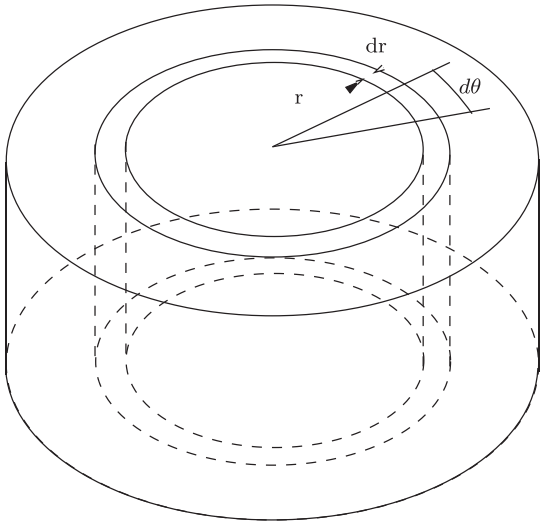

Fig. 1. Simplified model of the upset cylinder: the stresses are supposed to be equal in a slice.

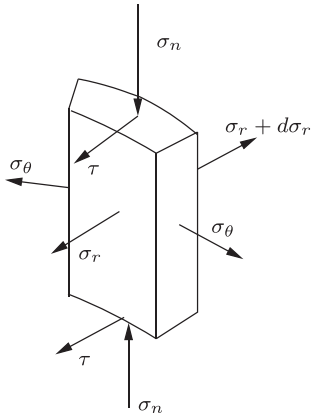

Fig. 2. Equilibrium of a slab.

Hence, replacing Eq. (3) and Eq. (4) into Eq. (2) and discarding terms higher than the first order, the equilibrium equation can be rewritten as:

$$rhd\sigma_r - 2\mu\sigma_n rdr = 0 \tag{5}$$

Since it is assumed that a plastic flow occurs, stresses verifies the relationship:

$$\sigma_n = \sigma_z = \sigma_0 - \sigma_r \tag{6}$$

where σ_0 is the yield stress. Finally, replacing this latest relation in Eq. (5), one gets:

$$\frac{h}{2\mu}\frac{d\sigma_r}{dr} + \sigma_r = \sigma_0 \tag{7}$$

Solving this ordinary differential equation for the boundary condition $\sigma_r(r_e) = 0$, r_e being the external radius of the cylinder, the solution is given by:

$$\sigma_r(r) = \quad \sigma_0\left[1 - \exp\left(\frac{2\mu}{h}(r_e - r)\right)\right] \tag{8}$$

$$\sigma_z(r) = \sigma_0 \exp\left(\frac{2\mu}{h}(r_e - r)\right) \tag{9}$$

These solution give some insight of the effects of a varying yield stress. Looking at Eq. (5), it can be deduced that radial stress is induced by the presence of the friction. This radial stress will

increase the normal stress (see Eq. (6)) and thus the friction force. Hence, letting the yield stress vary in the model also has an effect on the friction force.

Integrating on the interface on one of the dies the normal stress given in Eq. (8), one get the classical result for the forging load:

$$F = \frac{\pi r_e h}{\mu}\sigma_0 \left(\frac{e^A - 1}{A} - 1\right) \tag{10}$$

where we introduced $A = \frac{2\mu r_e}{h}$. In Eq. (10), the forging force relationship has been derived, which is the function of two parameters. First parameter is A which is combination of dimension and friction coefficients and the second is flow stresses σ_0. The parameter A is chosen such that forging force relationship is dependent only on the flow stresses σ_0 and that is reason that though friction coefficient exist in the model, it does not appear explicitly. Note that this result can also be extended to the case of a Tresca model of the friction force:

$$\tau = -\tilde{m}\frac{\sigma_0}{\sqrt{3}} \tag{11}$$

with $\tilde{m}$ the Tresca coefficient. Following the same approach, one finds that A in Eq. (10) is replaced by $A = \frac{2\tilde{m}r_e}{h}$.

Now, noticing that the forging load can be rewritten as a function of the height:

$$F(t) = \Psi(h(t))\,\sigma_0 \tag{12}$$

where the notation $h(t)$ is used to recall that the height of the sample is driven by the displacement of the die which will depend later on time, one can write the incremental strain as a function of $h(t)$:

$$\varepsilon(t) = 1 - \frac{h(t)}{h_0} \tag{13}$$

where h_0 is the initial height. Deriving the latest expression with respect to time, the strain rate is given by:

$$\dot{\varepsilon}(t) = -\frac{\dot{h}(t)}{h_0} \tag{14}$$

It is now possible to introduce a dependency of the yield stress to the vibration using a constitutive law i.e.:

$$\sigma_0(t) = \sigma_0\left[\varepsilon(t), \dot{\varepsilon}(t)\right] \tag{15}$$

thus, if one wants to describe a dependency of the yield stress on the vibration, the forging load can be expressed:

$$F(t) = \Phi\left(h(t)\right)\sigma_0\left[\varepsilon(t), \dot{\varepsilon}(t)\right] \tag{16}$$

Since this paper focuses on a viscoplastic material, this expression will be used in conjunction with a Norton–Hoff constitutive law which reads:

$$\sigma_0 = k\,\varepsilon^n \dot{\varepsilon}^m \tag{17}$$

where k is the consistency of material, n is a hardening coefficient and m is a sensitivity to strain rate. Note that no temperature term is considered. For the purpose of this study, which addresses cold forging and will focus on low frequencies, it is not required.

In next sections, the case of sinusoidal and triangular vibrations will be considered.

2.2. Sinusoidal vibrations

Replacing the Norton–Hoff law given by Eq. (17) into the expression (16) of the forging load yields:

$$F(t) = \Phi(h(t))\quad \varepsilon(t)^n \dot{\varepsilon}(t)^m \tag{18}$$

with $\Phi(t) = k\Psi(t)$.

To describe the movement of the dies, the height of the workpiece as a function of time is:

$$h(t) = h_0 + v_0 t + \frac{v_1}{2\pi f}\sin(2\pi f t) \tag{19}$$

where v_0 is the absolute value of the die's mean speed, $v_1 = 2\pi f a$ is the speed amplitude of the sinusoidal vibration which is superimposed (shown in Fig. 9), and f is the frequency in hertz. In this analytical model, vibration can be applied through any of the dies (upper or lower). Our main aim is to compress the cylindrical workpiece under the assumptions that workpiece will remain cylindrical and no thermal effects are present. From the expression (Eq. (19)), the speed of the die is written:

$$\dot{h}(t) = v_0 + v_1\cos(2\pi f t) \tag{20}$$

Note that the case of the upsetting at constant speed is also described by putting $v_1 = 0$ in the preceding equation. Hence, using Eq. (18), the expression of the forging load for no vibrations is given by:

$$F_0(t) = \Phi(\bar{h}(t))\quad 1 - \frac{\bar{h}(t)}{h_0}\quad^n \left[-\frac{v_0}{h_0}\right]^m \tag{21}$$

whilst in the presence of sinusoidal vibrations, the forging load is:

$$F_s(t) = \Phi(\tilde{h}(t))\quad 1 - \frac{\tilde{h}(t)}{h_0}\quad^n \left[-\frac{(v_0 + v_1\,\cos(2\pi f t))}{h_0}\right]^m \tag{22}$$

where the notations $\bar{h}(t)$ and $\tilde{h}(t)$ are introduced to distinguish the case where no vibrations and vibrations are applied respectively. Generally, the amplitude of the vibrations applied are small thus the following approximation holds:

$$\tilde{h}(t) \simeq h_0 - v_0 t = \bar{h}(t) \tag{23}$$

and as a consequence, it can also be deduced that:

$$\Phi(\bar{h}(t)) \simeq \Phi(\tilde{h}(t)) \tag{24}$$

leading to the following relationship between forces with and without vibrations:

$$F_s(t) \simeq F_0(t)\left[1 + \frac{v_1\cos(2\pi f)}{v_0}\right]^m \tag{25}$$

In order to evaluate effect of vibration, it is convenient to define the ratio $G = F_s/F_0$ which writes:

$$G(t) = \left[1 + \frac{v_1}{v_0}\cos(2\pi f t)\right]^m = \left[1 + R\cos(\omega t)\right]^m \tag{26}$$

where the ratio of speed $R = \frac{v_1}{v_0}$, and the frequency $\omega = 2\pi f$ are introduced. In order to ensure that the plastic flow is maintained, the sign of the rate of deformation should not change. As a compressive deformation is considered, it should thus always be positive or nil over a period of the vibration. By examination of Eq. (14), if $|v_1(t)| \le v_0$, the condition is respected. In the particular case of the sinusoidal vibration, this means that $0 \le R \le 1$. Actually, this condition is not strict, and the model could be extended to the case where $R > 1$ by letting the forging load being equal to zero in the time interval where $|v_1(t)| > v_0$, which would describe the fact that, since no elasticity is considered in the model, a loss of contact between the die and the workpiece would occur. This case will not be considered here. The ratio of Eq. (26) represents the forging load with vibration normalized with that without vibration. This expression indicates that:

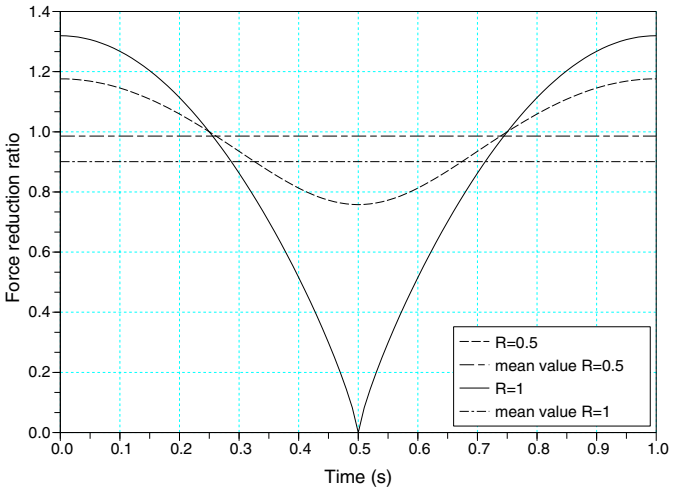

Fig. 3. Evolution of the force reduction ratio vs time at 1 Hz sinusoidal vibration.

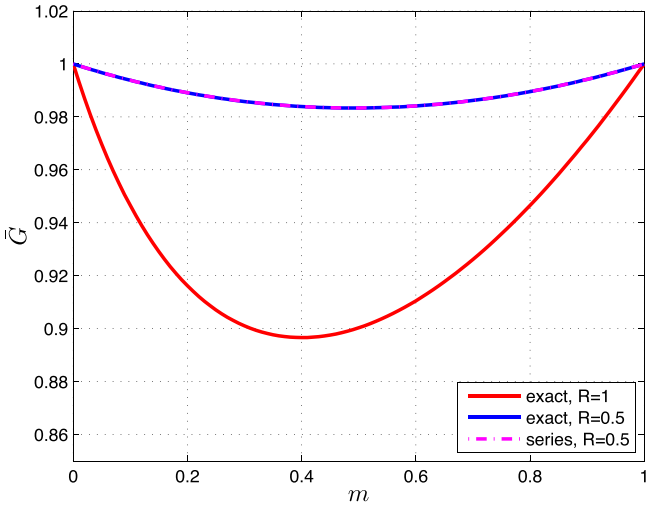

Fig. 4. Average value of the normalized forging load $\bar{G}$ as function of coefficient m.

- during the application of vibration, the forging load will oscillate over and under the value of that without vibration;
- the ratio is bounded by the values: $(1-R)^m \le G(t) \le (1+R)^m$ independently of the material consistency k and the hardening coefficient n;
- relative speed is a driving parameter of the forging load variation, and during the application of vibration, the forging load can be driven to zero if $R=1$ when the relative speed between the die and the workpiece is equal to zero;
- although the effect of friction exists in the model, the friction coefficient does not appear explicitly.

Fig. 3 illustrates the function $G(t)$ over one period (f=1 Hz, $m=0.4$) for the speed ratio $R=0.5$ and $R=1$. On the same figure, the mean value of the force reduction ratio is represented. From this, it can be concluded that the greater the speed ratio, the higher the benefit of the vibration (in the mean value). This is a consequence of the nonlinear form of the viscosity term in the Norton-Hoff law (where $m<1$), for in the process of calculating the mean, high strain rate have less weight.

From this observation, it can be concluded that in order to estimate the effectiveness of the vibration, the mean value of the normalized force is a better criterion. In the particular case $R=1$, an analytical solution can be established (Appendix A)[2]:

$$\bar{G} = -\frac{2^m \ \Gamma(m+0.5)}{\sqrt{\pi} \ \Gamma(m+1)} \tag{27}$$

For smaller speed ratio, an analytical solution can be also calculated in terms of special function[3]:

$$\bar{G} = (1+R)^m {}_2F_1\left[0.5, -m, 1, \frac{2R}{R+1}\right] \tag{28}$$

However, a series expansion is also possible provided that the relative speed is not too close to zero, where the derivative of $G(t)$ becomes singular:

$$\bar{G} = 1 + \frac{m(m-1)R^2}{4} + \frac{m(m-1)(m-2)(m-3)R^4}{64} + \frac{m(m-1)(m-2)(m-3)(m-4)(m-5)R^6}{2304} + o(R^8) \tag{29}$$

[2] The special function $\Gamma(x)$ is defined by $\Gamma(x) = \int_0^\infty t^{x-1}e^{-t}dt$.

[3] ${}_2F_1[a, b, c, y]$ is the Gauss hypergeometric function.

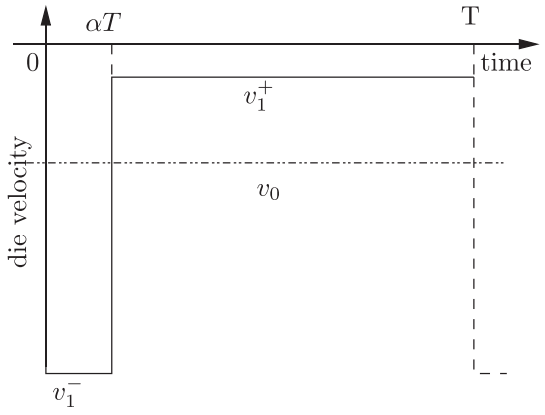

Fig. 5. Speed profile with duty ratio α.

Considering this equation, one conclude that the mean normalized forging load ratio $\bar{G}$ is a decreasing function of the speed ratio R, since only even power of this variable appears and the polynom has negative coefficients for powers greater than zero ($0 \le m < 1$).

It remains to study the dependency of $\bar{G}$ with respect to m ($0 < m < 1$). The curves obtained are represented Fig. 4. For comparison, the cases $R=0.5$ and $R=1$ were selected, and it confirms the property discussed before. The mean forging load reduction ratio has a minimum at $m=0.4$, where a reduction of nearly 10% occurs. From a practical point of view, values of m larger than 0.4 are rarely encountered and thus it can be concluded that in the case of sinusoidal vibrations, the force reduction is more important in the case of materials with a high dependency on strain rate.

2.3. Triangular vibrations

As already mentioned, due to the strain rate, the forging load oscillates between high and low values. However, the non linearity of the viscosity tend to mitigate the effect of high deformation rates. This is visible on Fig. 3 where the increase of the forging loads maximum values for $R=0.5$ and $R=1$ are close. In contrast, low speed will greatly reduce the stress. This suggests to use a different waveform which would alternate:

- during a large amount of the period at low speed v_1^+
- the rest of the period imposing a larger deformation rate by a high speed movement of the die (speed v_1^-).

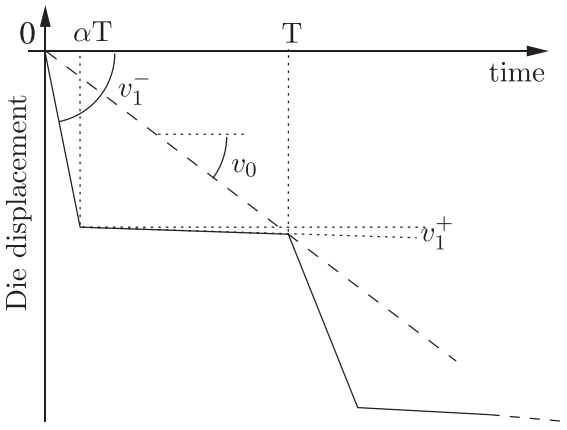

Fig. 6. Displacement triangular waveform with duty ratio α.

The simplest way to realize these requirements is to use a square waveform with a variable duty ratio α for the speed. Fig. 5 illustrates such a die velocity profile. The resulting (upper) die displacement is represented on Fig. 6 which is a triangular waveform with constant drift. In case of triangular vibration, a high vibration velocity is applied in downward direction for a small time to support the forging direction and for long time, low velocity is applied in upward direction thus greatly reducing the stress produced due to opposite velocity. But the vibration high velocity in downward direction to support forging cannot be applied for a long time and it can be a problem in practice for this would imply the use of high dynamic auxiliary actuators to realize the vibration. The slope of the drift corresponds to the mean speed v_0 given by the equation:

$$v_0 = \frac{1}{T}\int_T v(t)dt = \alpha v_1^- + (1-\alpha)v_1^+ \tag{30}$$

Introducing the amplitude of the square wave $A = v_1^+ - v_1^-$, the previous equation can be rewritten:

$$v_0 = \frac{1}{T}\int_T v(t)dt = v_1^- + (1-\alpha)A \tag{31}$$

Most of the benefits of the proposed strategy will be attained if $v_1^+ = 0$, leading to $v_1^- = -A$ and then:

$$v_0 = -\alpha A \tag{32}$$

which shows that two "design" parameters are left for the speed waveform.

With such a speed waveform, the expression of the mean force reduction is remarkably simplified:

$$\begin{aligned}\bar{G} &= \frac{1}{T}\int_0^T G(t)\,dt = \frac{1}{T}\int_0^T \left(\frac{v_1(t)}{v_0}\right)^m dt \\ &= \frac{1}{T}\int_0^{\alpha T}\left(\frac{v_1^-}{v_0}\right)^m dt + \frac{1}{T}\int_{\alpha T}^T \left(\frac{v_1^+}{v_0}\right)^m dt\end{aligned} \tag{33}$$

$$= \left(\frac{v_1^-}{v_0}\right)^m \alpha + \left(\frac{v_1^+}{v_0}\right)^m (1-\alpha) \tag{34}$$

Using the assumption $v_1^+ = 0$ (limit of unloading), the expression simplifies to:

$$\bar{G} = \alpha\left(\frac{v_1^-}{v_0}\right)^m$$

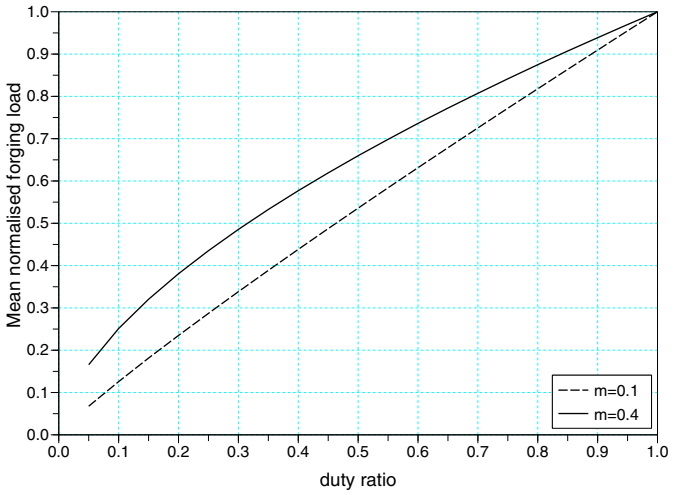

Fig. 7. Effect of duty ratio α on the mean normalized forging load G.

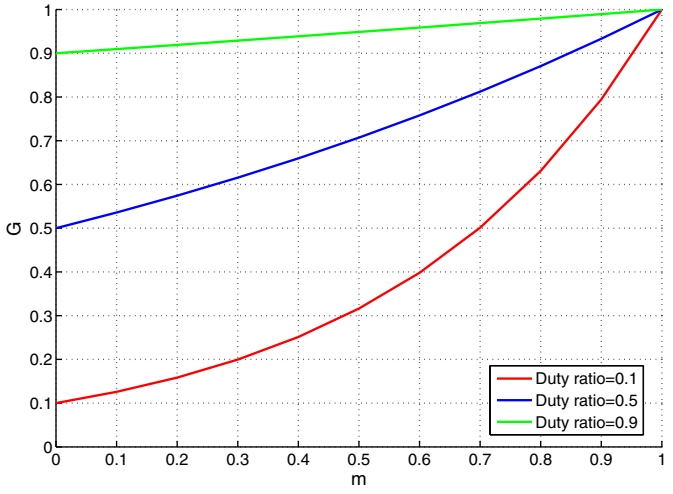

Fig. 8. Effect of strain rate sensitivity m on the mean normalized forging load G, $\alpha = 0.1$, 0.5 and 0.9.

Replacing the expression Eq. (32), the mean force reduction ratio is given by:

$$\bar{G} = (\alpha)^{1-m} \tag{35}$$

From this relation, since $0 < m < 1$, it can be deduced that the smaller the duty ratio the larger will be the reduction of the forging effort as Fig. 7. Another "surprising" conclusion is that, using this model, optimising the velocity waveform leads to a strategy somewhat similar to incremental forging processes. Fig. 8 shows the mean force reduction ratio for α = 0.1, 0.5 and 0.9 versus the sensitivity to strain rate m. Contrarily to the case of sinusoidal vibrations, the material with lower viscosity perform better, and the reduction of the effort can theoretically reach values as high as 90 %.

3. Finite Element modeling and simulation of forging process with vibration

The main features of the model is that the mean value of the normalized forging load:

- remains constant along the process
- does not depend on the material consistency and its hardening coefficient

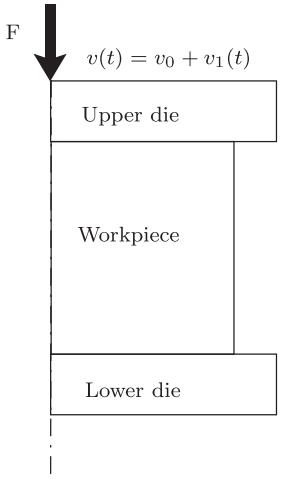

Fig. 9. Schematic of the model used in FORGE 2008: the upper die is moving and the lower die is fixed. The upper die's velocity is obtained by adding the vibration speed $v_1(t)$ is added to the usual constant velocity v_0.

- does not depend on the friction coefficient
- does not depend on the geometry in the case at hand

However, these properties could be a consequence of the assumption on the material flow that underlie the model. In practice, the material is not only flowing radially and the stresses are more complicated under the influence of friction effects which result in the barreling of the workpiece. Hence, although the model does take into account friction as shown in Section 2, their effect on the geometry are ignored by the model.

The main objective of this section is to use finite element method (FEM) software Forge® simulations of the forging process including vibrations to validate the proposed analytical model. The simulation parameters were chosen as close as possible to the assumption underlying the model, in order to evaluate the influence of the kinematic both in the case of sinusoidal and triangular vibrations waveforms. For the different configurations, the vibrations were simulated by imposing the upper die speed as depicted in Fig. 9. This choice is imposed by the software used which can only simulate a movement of the lower die using data stored in a file. In the case of vibration, such a file becomes rapidly huge and disk access considerably slows the simulation down. As for the upperdie a fortran routine can be used and that no differences between the two approaches could be noticed from preliminary simulations, this solution was adopted. In the simulations presented here, v_0 was equal to 3 mm s^{-1}, which was the speed used for experiments (Ly et al., 2009).

3.1. Simulation protocol for sinusoidal vibrations

The analytical model shows that the maximum gain is obtained for a unitary speed ratio, hence the value of v_1 is chosen such that the frequency f and amplitude a of the sinusoidal vibration respect the relationship $2\pi af = v_0$. Low frequencies were used in the range of 40–125 Hz, the amplitude being calculated accordingly.

The simulation were first undertaken assuming a pure visco-plastic behaviour. Consistency K and hardening coefficient n of the material were kept constant, while the sensitivity of strain rate m was varied in the range of 0.1–0.9 to compare it with the analytical model. Thermal effects were cancelled, and the friction is modelled using a tresca model with $\bar{m} = 0.8$. Table 1 summarizes the different parameters of the simulation as well as the geometry of the workpiece used. Simulations were performed to analyze other parameters such as n and k to see the impact of vibration on metal forming process but no or limited gain in forming force reduction was observed.

Table 1
FEM Model description for the forging process.

Workpiece material	$k = 161.9$ MPa, $n = 0.2$
	$0.1 \leq m \leq 0.9$
Tresca friction coefficient	$\bar{m} = 0.8$
Workpiece diameter	40 mm
Workpiece initial height	40 mm
Workpiece final height	15 mm
Simulation model	Axisymmetric
FEM software	FORGE 2008®
Die	Non deformable (Rigid)
Die mean velocity	3 mm s^{-1}
Workpiece Meshing	Triangular
Time step (with vibrations)	0.25 ms (fixed)
Time step (without vibration)	25 ms (fixed)

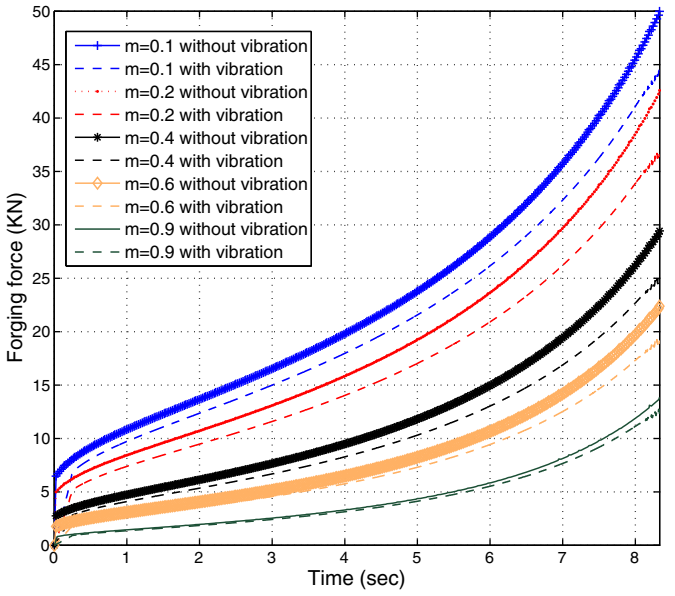

Fig. 10. Influence of the strain rate sensitivity m on the forging process for sinusoidal vibrations $v = 3$ mm s^{-1}, $f = 40$ Hz and $a = 12$ μm.

On Fig. 10, some of the average forging load vs time simulated with and without vibrations for different values of m are presented. In the case when vibrations were applied, the results obtained from the simulation present large oscillations. The curves were therefore filtered using a moving average filter of ten periods. This figure clearly shows the expected effect of forging load reduction with the application of vibrations i.e. the dependency on m and the constant ratio between the forging load with and without vibrations. These results will be discussed more in depth in the result section.

3.2. Simulation of triangular vibrations

The parameters summarized in Table 1 were also used for the case of triangular vibrations. The simulations were all performed using a duty ratio $\alpha = 0.1$. Theoretically, the displacement should be simulated using a periodic (T being the period) piecewise constant speed function imposing a velocity of 30 m s^{-1} during αT, the die being at rest during the remaining time (i.e $v_1^+ = 0$). However, with such a speed profile, the simulator automatically stops due to zero detection problems. therefore a slightly higher speed had to be used, in order to have a separation of the die and the workpiece and thus prevent such inappropriate ending of the calculations. Such simulations being time-consuming the value for m only spanned the range 0.1–0.4 which covers most of the actual material range.

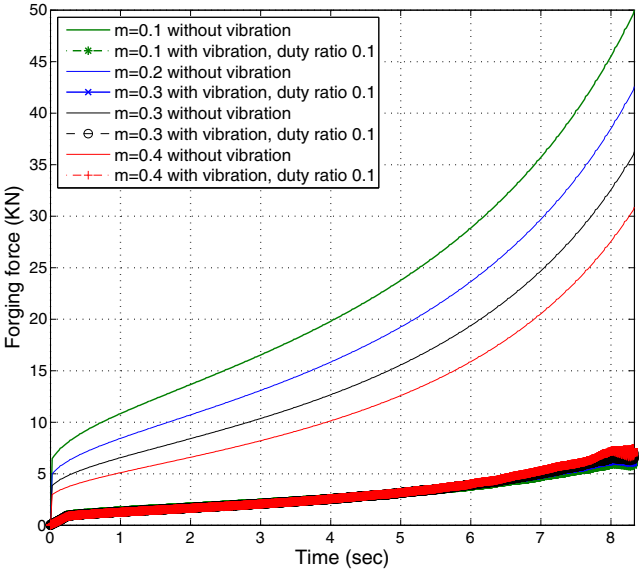

Fig. 11. Effect of strain rate sensitivity on the forging process for triangular vibrations ($v = 3\,\text{mm s}^{-1}$, $f = 40\,\text{Hz}$ $a = 67.6\,\mu\text{m}$).

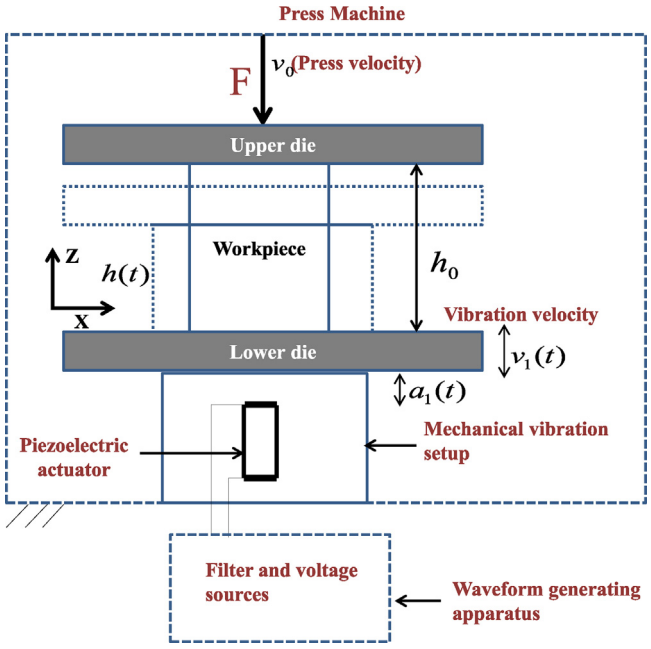

Fig. 12. Schematic of vibration setup used for vibration assisted forging.

Some of the results for such simulations are presented on Fig. 11. Again the results of simulation are filtered to remove the oscillation using a moving average filter. The figure clearly shows the significant reduction of the mean forging load and the constant ratio between loads with or without vibrations.These results are quite striking as compare to results presented for sinusoidal vibration assisted forging process. In case of sinusoidal vibration (Fig. 10), time for signal going up and down are equal. During the time in which die direction and vibration direction are same, forging force to deform the workpiece is reduced but for the same duration of time when die and vibration direction are opposite, it cause increase in forging force and stresses. However low speed vibration in upward direction will greatly reduce the stress in the workpiece and that is what happened physically while applying triangular vibration. In case of triangular vibration, we apply very high vibration velocity in downward direction for a small time to support the forging direction and for long time applied low velocity in upward direction thus greatly reducing the force and stress produced due to two opposite velocity (Fig. 11).

4. Experimental validation of analytical model

The experiments of conventional forging and vibration assisted forging processes were performed on two different compression machines Lloyd LR30K and ZWICK Roell Z1200. Lloyd machine is less rigid and was used for forging of plasticine workpieces. ZWICK Roell Z1200 is more rigid and was used for the forging of aluminium workpieces. Schematic of vibration assisted forging process is shown in Fig. 12. Three main parts of the vibration assisted forging process as presented in Fig. 12 are

- Press machines with max force capacity at full speed:
  Lloyd LR30K (30 kN) and ZWICK Roell Z1200 (1200 kN)
- Special mechanical setup incorporating piezoelectric actuator to transfer the vibration to lower die
- Waveform generating apparatus

Special mechanical setup or vibration pot allows the vibration generation to be transferred in the specific direction. The piezoelectric actuator has been integrated in an elastic system to vibrate the lower die. Stack piezoelectric actuators were selected since the application needs a vibrating device that delivers large forces (up to 20 kN in the tests), small vibration amplitudes (maximum amplitude 20 μm in these tests), and frequencies up to 125 Hz. In order to avoid mechanical damage of the piezoelectric actuator, the force applied to it during the process should only acts on its longitudinal axis and should only be compressive. The power supply is designed to generate high voltage waveform from a standard continuous voltage power supply (Table 2).

Table 2
Description of the devices used to measure and generate vibration.

Displacement sensor	Heidenhain *MT*2581
Counter card	Heidenhain *IK*220
Force sensor	Kistler 9351*B*
WCharge amplifier	Kistler 5015*A*
Current sensor	LEM *PR*30
Voltage sensor	LEM *LV*25
Piezoelectric actuators	PZT 1000/35/40 or PZT 1000/16/60
Acquisition card	NI 6124

Different types of waveforms obtained from the experimental setup are shown in Fig. 13 though sinusoidal and triangular vibrations are used only in this article. Normal waveform were used to see the influence of a wave with the speed's change faster than sinusoidal but still smooth rather than non-continuous in the case of triangular or square waveforms. It can be seen from the Fig. 13 that it is difficult to obtain perfect triangular and square waveform due to the system dynamics and they were slightly distorted but were still useful to be used in experiments

4.1. Experiments for forging process without vibration

First, identification of material parameters for a cylindrical plasticine workpiece was performed. These material parameters have already been mentioned in Section 2 while describing Norton-Hoff law of material behavior and are recalled here:

k = Consistency of material,
n = Material hardening coefficient,
m = Coefficient of sensitivity to strain rate

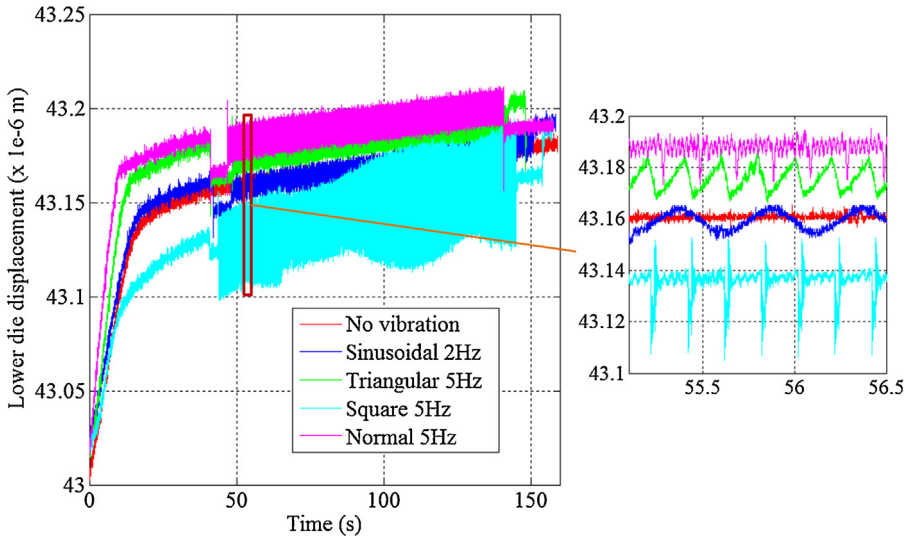

Fig. 13. Different types of waveforms applied in forging process.

Table 3
Geometry and process parameters.

Workpiece material	Plasticine
Workpiece dimension	Diameter 50 mm, Height 51 mm
Die material	Steel
Upper die displacement	25 mm

Table 4
Geometry and process parameters.

Material coefficients	Plasticine	Aluminum
n	0.125	0.45
m	0.116	0.05
k	289 kPa	247 MPa
$\bar{m}$	0.08	0.0005
K_e/E	3.5 kN/m, 90.2 kPa	95 MN/m, 31.6 GPa

Table 5
Geometry and process parameters of forging process with sinusoidal vibration.

Workpiece material	Plasticine
Workpiece dimension	Diameter 30.2 mm, Height 30.4 mm
Upper die velocity	2.5 mm s^{-1}
Vibration frequency	50 Hz
Voltage (peak to peak)	400 V
Amplitude (peak to peak)	18 μm

In this case, two experiments of forging tests were performed without applying vibration. These tests were performed with two different press velocities $v_0 = 0.5\,\text{mm s}^{-1}$ and $4\,\text{mm s}^{-1}$ for the same dimensions of the plasticine samples. Other parameters used in calculation are given in Table 3.

Force versus die displacement curves are obtained experimentally and optimization criteria was employed to find the material and friction parameters as adopted by Ly et al. (2009). The material and friction parameters obtained from these steps while using plasticine as workpiece are presented in Table 4. Similarly, Material and process parameters were determined for aluminum from other experiments are also presented in Table 4.

Similarly, Material and process parameters were determined for aluminum.

4.2. Experiments for forging process with sinusoidal vibration

Experiment for upsetting a cylindrical plasticine workpiece was performed where vibration and no vibration are applied during one experiment. The comparison is made between the part of force with and without vibration. Initially, upset forging was started without applying vibration and after some time sinusoidal vibrations were applied. The amplitude applied in this case was determined by displacement sensor which corresponds to 18 μm. Geometry and process parameter for this experiments are given in Table 5.

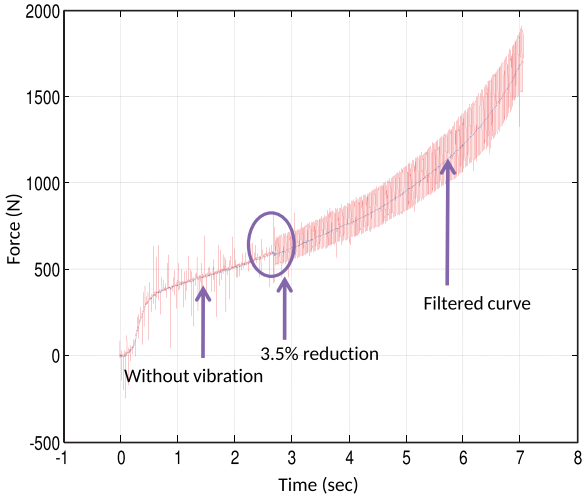

Fig. 14. Force versus time for a upset forging of plasticine in presence of sinusoidal vibration ($v_0 = 2.5\,\text{mm s}^{-1}$, $f = 45$ Hz and $a = 18$ μm).

In this case, Velocity ratio = $R = v_1/v_0 = 1$. The force curve is plotted against time and is presented in Fig. 14.

There is a reduction of nearly 3.5% in this case. From the analytical model for $m = 0.116$, the gain in forging force reduction is nearly 5%, so our result is well in the domain of analytical model.

Due to the stiffness problem related to Lloyd machine LR30K, it was preferred to perform the upsetting forging of aluminium on the Zwick Roell Z1200 testing machine with a maximum load capacity of 1200 kN. Geometrical and process parameter for sinusoidal vibration assisted upsetting forging process for aluminium is presented in Table 6.

Force curve has been presented in Fig. 15 for the forging process with sinusoidal vibrations. The case is important in a sense that we have chosen velocity ratio as $R = 1$ to compare it with the analytical model. The amplitude use in case of analytical model is average amplitude and not peak to peak, so for $R = 1$, amplitude of 2 μm is used.

Table 6
Geometry and process parameters of forging process with sinusoidal vibration for aluminum.

Workpiece material	Aluminum
Workpiece dimension	Diameter 8 mm, Height 16 mm
Upper die velocity	1.5 mm s^{-1}
Vibration frequency	2 Hz
Voltage (peak to peak)	500 V
Amplitude (peak to peak)	4 μm

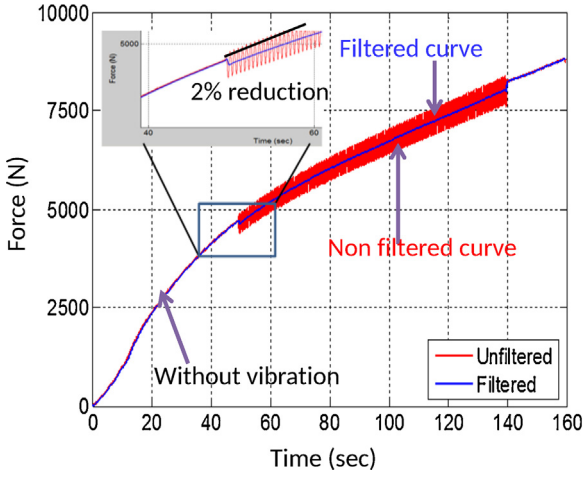

Fig. 15. Force versus time for a upset forging of aluminum in presence of sinusoidal vibration ($v_0 = 1.5$ mm s^{-1}, $f = 2$ Hz and $a = 4$ μm).

Table 7
Geometry and process parameters of forging process with triangular vibration for plasticine.

Workpiece material	Plasticine
Workpiece dimension	Diameter 31 mm, Height 30.2 mm
Upper die velocity	0.25 mm s^{-1}
Vibration frequency	15 Hz
Voltage (peak to peak)	400 V
Amplitude (peak to peak)	17 μm
Duty ratio (α)	0.9

From Fig. 15, it can be seen that there is reduction of 2.0% forging force for the forging process when sinusoidal vibration has been applied. The force curve is filtered using moving average over 1000 points determined from the frequency of vibration and sampling. Gain can be compared with the analytical model presented in Fig. 3 for $m = 0.05$. It is approximately 2% which is in accordance with the experimental results.

4.3. Experiments for forging process with triangular vibration

In order to analyze the advantage of using new waveform, triangular waveform is chosen to be used during the upset forging. It was discussed earlier in the case of sinusoidal vibration assisted forging process that forging forces reduces when the vibration and die velocity are in the same direction. In case of sinusoidal vibration, time of wave going upward and downward is same and we can not control it. Theoretically, use of triangular vibrations gives the advantage of control of signal duty time (α) and signal going up time can be reduced.

Experiment with triangular vibration assisted upset forging were performed with plasticine. Geometrical and process parameters for this experiment are shown in Table 7.

Triangular vibrations were applied and removed during certain periods during the experiment. Force curve for this process has been shown in Fig. 16.

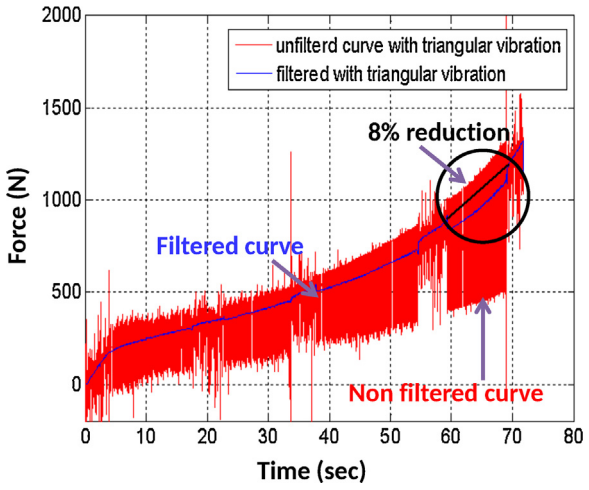

Fig. 16. Force versus time for a upset forging of plasticine in presence of triangular vibration ($v_0 = 0.25$ mm s^{-1}, $f = 15$ Hz, $a = 19$ μm) and $\alpha = 0.9$.

There is a decrease of 8% in forging force at the end of the process. That is lower than what is predicted by the analytical model as given by Eq. (35) and Fig. 11. As For $m = 0.116$ (plasticine) and $\alpha = 0.9$, there is a theoretical gain of 8.9% slightly more than expected from the model. The deviation of the experimental results for triangular vibration assisted forging process from the analytical model can be attributed to two facts:

- The relaxation time for the material is very small for this time period, he material is not properly relaxed and the vibration is applied again meanwhile thus the gain in forging force reduction is not as it was expected.
- Effect of elasticity cannot be neglected.

The true gain of forging force reduction for triangular vibration given by the analytical model is verified with the help of square velocity waveform generated by simple incremental forging process on the Llyod machine. Initially, upper die is moved downward with the constant velocity $v_1^- = 3$ mm s^{-1} and then it is stopped $v_1^+ = 0$ mm s^{-1}. The material is given some time (0.5 s) to relax then upper die moves again, thus reducing the plasticine ($m = 0.116$) workpiece height with each increment. This type of forging process is possible by programming die travel in the Lloyd machine. The duty ratio for incremental forging process was calculated by signal going up time to time period of the signal and was found to be 0.66 in this case. The gain for the process was calculated by Eq. (35) which is 0.68. The process is compared with the simple forging process with $v_o = \alpha v_1^- = 2.1$ mm s^{-1} and is presented in Fig. 17.

The gain obtained from analytical model and the comparison of two curves are very close to each other which confirm our reasoning that material was not given enough time to relax during experiments to obtain the true gain in forging force reduction.

5. Results and discussion

An important feature of the model is that the sensitivity to strain rate m is a key parameter in the force reduction. The FEM simulations also confirms the considerable impact of the proposed waveform, which is also illustrated by Fig. 18 where all the results are superimposed. For sine waveforms, Fig. 18 represent the mean force reduction ratio against predicted by the analytical (full line) and FEM (dots) models. Each dot corresponds to a simulation. Clearly they follow the same shape as the curve of the analytical but the simulation predict a mean reduction ratio of 4% less than the proposed model.

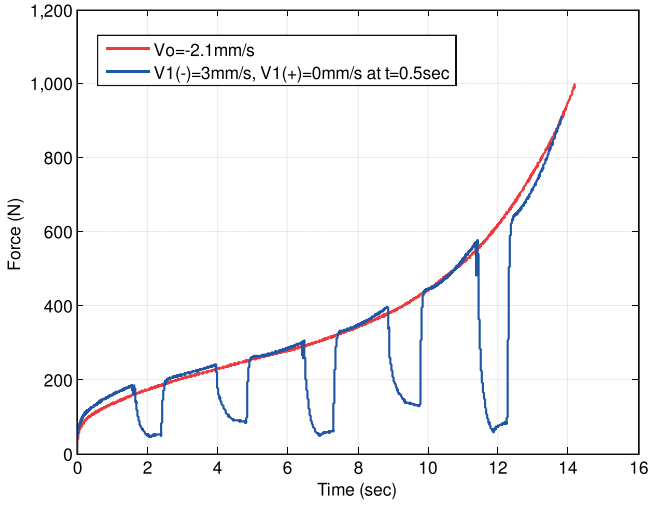

Fig. 17. Comparison of forging process with $v_o = \alpha v_1^- = 2.1\,\mathrm{mm\,s^{-1}}$ and superimposed triangular vibration.

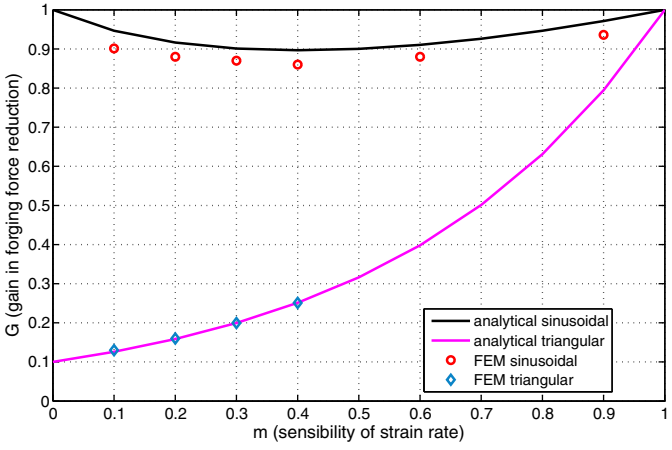

Fig. 18. Comparison of normalized forging load for sinusoidal and triangular vibrations.

From the experiments for sinusoidal vibration assisted forging process for plasticine and aluminum, gain obtained coincides with what predicted by analytical model. In the case of triangular waveforms, the comparison is also presented on Fig. 18. The analytical model is in much better agreement this time with a relative error between the two models always less than 1%. In case of experiments performed for triangular vibration assisted forging process of plasticine, the results are closer to what predicted by analytical model and reason of deviation are material relaxation time and elasticity. The two advantages of using such a waveform over a sinusoidal one become clear: more reduction on the forging load in the mean value is obtained, and the effect is an inverse sensitivity to the coefficient m which allow to apply it even to cold forging.

The discrepancy between the FEM and the analytical models in the case of sine vibration waveforms may be explained in the light of the result of the triangular waveform. Since the same model is used in both cases, the only difference is the speed profile used. The dynamic effects are not considered in the analytical model. However, they are more important in the case of the sinusoidal die speed as they are present over a whole period, as opposed to the case of triangular waveform where acceleration appears only briefly at the transition in the speed waveform. This suggest that the model is not suitable at high frequencies.

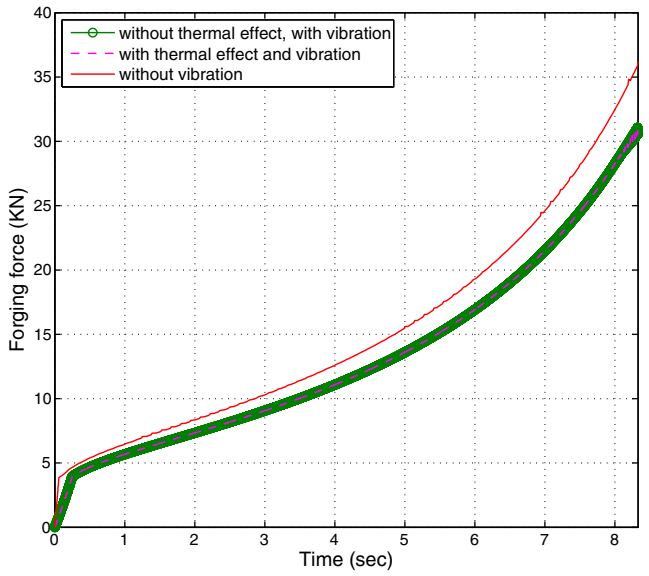

Fig. 19. FEM prediction of the forging load for sinusoidal vibrations with thermal effects.

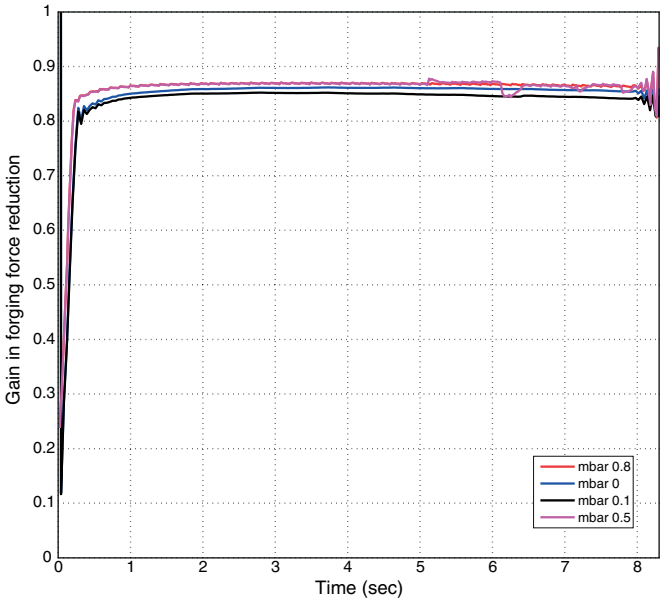

Fig. 20. Normalized mean forging load $\bar{G}$ for a sinusoidal vibrations (40 Hz)and different Tresca friction coefficients. The sensitivity to strain rate is 0.4 for these simulations.

Among the simplifying assumptions, the thermal effects were ignored. However, they could be also influencing the forging process by inducing a thermal gradient at the die-workpiece interface. In order to verify this, some supplementary simulations including a thermal term in the Norton-Hoff law were done. The results presented in Fig. 19 with $m = 0.4$. No evidence of a thermal dependency can be noticed and from the simulation only an increase of a few degrees were calculated. This should not lead to the conclusion that they have no influence, but that they can be neglected for the frequencies considered in this work.

Similarly, impact of Tresca friction coefficient on gain in forging force reduction is also analyzed with the help of FEM simulations. On Fig. 20, a typical result of the normalized forging load reduction is represented.

The curves are almost constant. The variations at the beginning and the end of the simulation are after effects of the filtering process

Table 8
Dependence of $\bar{G}$ on $\bar{m}$.

$\bar{m}$	0	0.1	0.5	0.8
$\bar{G}$	0.86	0.84	0.87	0.87

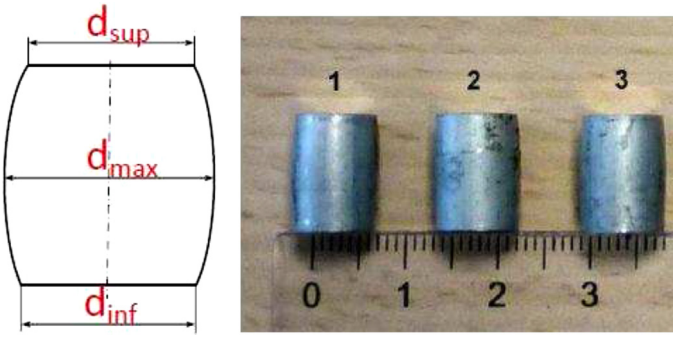

Fig. 21. Barreling effect in copper under 1. no vibration, 2. sinusoidal and 3. triangular vibrations.

(a moving average filter as mentioned earlier). For all the simulations performed the properties pointed out in Section 3 were verified. This seems to indicate that the influence of barrelling is not dominating. In this model, homogeneous strain has been considered and distribution of stresses depends only on the radius of workpiece. It is a fair assumption for this simple case. On the same figure, different $\bar{m}$ were used in order to demonstrate the weak dependency of the forging load reduction on the friction coefficient value. The results of the mean of $\bar{G}$ on an interval around $t = 4$ s summed up in Table 8 show a little variation when varying $\bar{m}$ as expected.

During experiments, the barreling effect is analyzed for the copper workpiece as shown in Fig. 21. The result of forging force reduction for copper is not presented here as copper showed the influence of elasticity and another model for elastic visco-plastic domain has been developed.

This is done by measuring d_{max} (barreling), d_{sup} (upper surface diameter), d_{inf} (lower surface diameter) and comparing their ratios for no vibration, sinusoidal and triangular vibration. The application of vibration effectively reduce the effect of "barreling" in comparison to without vibration thus indicating a tribological effect. This is somehow deviation from our model assumption that assume no barreling effect. Thus in real life, some of the assumption made during the method of slice are violated.

Acknowledgements

The authors would like to thank Dr Tudor Balan for his remarks and Mr Luc Morhain for his technical support. This project was supported by the GI2M Fédération de Recherche of the Paul Verlaine University of Metz. The authors would also like to thank Higher Education Commission (HEC) of Pakistan for the PhD scholarship funding.

Appendix A.

In order to find the exact solution of Eq. (26) we substitute,

$$y = (1 + R\,Cos(\omega t))$$
$$dy = -\omega R \sin t(\omega t)dt$$
$$dy = -\omega \quad \overline{R^2 - (y-1)^2}$$

And the limit will be transformed i.e. at $t = 0$, $y = 1 + R$ and at $t = T/2$, $y = 1 - R$. Eq. (26) will now become,

$$\bar{G} = \frac{-2}{T\omega}\int_{1+R}^{1-R} \frac{y^m}{\overline{R^2 - (y-1)^2}}dy = \frac{-1}{\pi}\int_{1+R}^{1-R} \frac{y^m}{\overline{R^2 - (y-1)^2}}dy$$

The exact solution of above integral can now be calculated for a special case of $R = 1$ using Mathematica tool. The results are,

$$\bar{G} = \left| \frac{1}{\pi} 2\frac{1}{2} + m \quad \overline{2 - y}\text{Hypergeometric2}F1\left[\frac{1}{2}, \frac{1}{2} - m, \frac{3}{2}, 1 - \frac{y}{2}\right]\right|_2^0$$

$$\bar{G} = \frac{2^m}{\sqrt{\pi}} \frac{\text{Gamma}(m + 0.5)}{\text{Gamma}(m + 1)}$$

References

Presz, W., Andersen, B., 2007. Flexible tooling for vibration-assisted microforming. J. Achiev. Mater. Manuf. Eng. 21, 61–64.
Blaha, F., Langenecker, B., 1959. Ultrasonic investigation of the plasticity of metal crystals. Acta Metall. 7, 93–100.
Lehfeldt, E., 1969. Influence of ultrasonic vibration on metallic friction. J. Acoust. Soc. Am. 45, 334–335.
Mousavi, S., Feizi, H., Madoliat, R., 2007. Investigations on the effects of ultrasonic vibrations in the extrusion process. J. Mater. Process. Technol. 187, 657–661.
Rosochowska, M., Rosochowski, A., 2007. Fe simulation of ultrasonic back extrusion. AIP Conf. Proc. 907, 564–569.
Kumar, V., Hutchings, I., 2004. Reduction of the sliding friction of metals by the application of longitudinal or transverse ultrasonic vibration. Tribol. Int. 37, 833–840.
Lucas, M., Daud, Y., 2009. A finite element model of ultrasonic extrusion. J. Phys. Conf. Ser. 181, 012027.
Kaiyuan, C., Nanqiao, Z., Bin, L., Shengping, W., 2009. Effect of vibration extrusion on the structure and properties of high-density polyethylene pipes. Polym. Int. 58, 117–123.
Siegert, K., Ulmer, J., 2000. Superimposing ultrasonic waves on the dies in tube and wire drawing. J. Eng. Mater. Technol. 123, 517–523.
Siegert, K., Ulmer, J., 2001. Influencing the friction in metal forming processes by superimposing ultrasonic waves. CIRP Ann. Manuf. Technol. 50, 195–200.
Murakawa, M., Jin, M., 2001. The utility of radially and ultrasonically vibrated dies in the wire drawing process. J. Mater. Process. Technol. 113, 81–86.
Hayashi, M., Jin, M., Thipprakmas, S., Murakawa, M., Hung, J.-C., Tsai, Y.-C., Hung, C.-H., 2003. Simulation of ultrasonic-vibration drawing using the finite element method (fem). J. Mater. Process. Technol. 140, 30–35, Proceedings of the 6th Asia Pacific Conference on materials Processing.
Ashida, Y., Aoyama, H., 2007. Press forming using ultrasonic vibration. J. Mater. Process. Technol. 187–188, 118–122, 3rd International Conference on Advanced Forming and Die Manufacturing Technology.
Polyakov, N., Mikhailov, N., 1967. A study of vibration-assisted deformation of metals. Mater. Sci. 2, 346–347.
Huang, Z., Lucas, M., Adams, M., 2000. Modelling wall boundary conditions in an elasto-viscoplastic material forming process. J. Mater. Process. Technol. 107, 267–275.
Huang, Z., Lucas, M., Adams, M., 2002. Influence of ultrasonics on upsetting of a model paste. Ultrasonics 40, 43–48.
Daud, Y., Lucas, M., Huang, Z., 2007. Modelling the effects of superimposed ultrasonic vibrations on tension and compression tests of aluminium. J. Mater. Process. Technol. 186, 179–190.
Hung, J., Hung, C., 2005. The influence of ultrasonic-vibration on hot upsetting of aluminum alloy. Ultrasonics 43, 692–698.
Hung, J.-C., Tsai, Y.-C., Hung, C., 2007. Frictional effect of ultrasonic-vibration on upsetting. Ultrasonics 46, 277–284.
Ly, R., Giraud-Audine, C., Abba, G., Bigot, R., 2009. Experimentally valided approach for the simulation of the forging process using mechanical vibration. Int. J. Mater. Form. 2, 133–136.
Lange, K., 1985. Handbook of Metal Forming. McGraw-Hill.